Tutor
Dr. Francesc Centellas Masuet
Departament de Química Física

Grau de Química

Treball Final de Grau

Study of the degradation of monoazo dye Acid Red 1 using electrochemical anodic oxidation, electro-Fenton and photoelectro-Fenton processes.

Estudi de la degradació del colorant monoazoic Acid Red 1 emprant processos electroquímics d'oxidació anòdica, electro-Fenton i fotoelectro-Fenton.

Xavier Florenza Garcia

January, 2014

Universitat de Barcelona
Campus d'Excel·lència Internacional B:KC Barcelona Knowledge Campus

El grau de química ha suposat un llarg i dur camí per a mi. Ara que ja s'acaba, m'agradaria recordar primerament als meus pares, Josep i Núria, sempre fent-me costat en quasevol circumstància; recordar també a totes aquelles persones que m'he anat trobant durant tot aquest temps i m'han ajudat fent el camí més plàcid: Judith, Pau, Helios, Foix, Anna, Jordi, Martí, Ronald, Jordi, Ana, Carles, Sandra, Carla, Berta, Núria, Basso, Eloi, Anna, Montse i Alba, gràcies. I a la Dra. Elvira Gómez, és clar, també gràcies.

M'agradaria agrair a l'Abdu, Fabio, Griselda, Gabriel, Nelly i Laye, membres del laboratori d'Electroquímica de Materials i del Medi Ambient, la seva companyia durant el procés en que ha esdevingut aquesta memòria, i fer una menció especial per a en Sergi Garcia i l'Aline Sales, que m'han guiat, m'han ajudat i m'han aguantat.

Per últim, voldria agrair els consells, els ànims i la feina de'n Francesc Centellas, el tutor d'aquesta memòria, de qui només se'n pot aprendre. A tots vosaltres, moltes gràcies.

REPORT

CONTENTS

1. SUMMARY

A comparative study of the degradation of the monoazo dye Acid Red 1 (AR1) was carried out to elucidate the effectiveness of electrochemical anodic oxidation (AO), electro-Fenton (EF) and photoelectro-Fenton (PEF) processes, three representatives of the so-called electrochemical advanced oxidation processes (EAOPs).

Three different aspects were taken into account in order to assess degradation levels achieved, i.e. mineralization, decolouration and species released into the solution. Electrolytic trials were performed using an air-diffusion PTFE/carbon cathode and Pt or boron-doped diamond (BDD) anodes alternately, the latter yielding the best performance.

The mineralization level was quantified through the electrolytic processes by means of total organic carbon (TOC) measurements. PEF process performs the best in mineralization terms. EF follows with a medium-high performance while AO proves to be the least effective process, especially when Pt anode is used.

Spectrophotometric measurements allowed decolouration monitoring. EF and PEF processes present the same behaviour, reaching complete decolouration in minute-scale. AO has a poorer performance; decolouration is completed after several hours of electrolysis or, in some cases, not even achieved.

Short-chained carboxylic acids and inorganic ions were detected and quantified through HPLC techniques. Oxalic and oxamic acids are the main carboxylic species found in EF and PEF processes, while only low concentrations are noticed in AO. NH_4^+, NO_3^- and SO_4^{2-} ions are found in solution. NH_4^+ is the majority inorganic *N*-specie in EF and PEF processes; NO_3^- is it in AO. All sulphur atoms contained in AR1 are released as SO_4^{2-} for all the three methods assessed.

The main conclusion is that EAOPs tested stand as clean, easy and powerful processes to degrade complex aromatic molecules like AR1.

Keywords: electrochemical advanced oxidation processes, electro-Fenton, photoelectro-Fenton, anodic oxidation, water treatment, boron-doped diamond, Acid Red 1.

2. RESUM

Es va dur a terme un estudi comparatiu sobre la degradació del colorant monoazoic Acid Red 1 a través de tres mètodes representatius dels anomenats processos electroquímics d'oxidació avançada (EAOPs): procés d'oxidació anòdica (AO), procés electro-Fenton (EF) i procés fotoelectro-Fenton (PEF).

Tres aspectes diferents es van tenir en compte per evaluar els nivells de degradació aconseguits per cada un d'ells: mineralització, decoloració i espècies alliberades a la solució. Els experiments electrolítics es van realitzar fent servir un càtode de PTFE/carboni de difusió d'aire i ànodes de Pt o diamant dopat amb bor (BDD) alternativament, sent aquest últim el més eficaç.

El nivell de mineralització durant les electròlisi va ser quantificat a través de mesures de carboni organic total (TOC). El procés PEF rendeix els millors resultats, seguit pel procés EF, amb un nivell de mineralització mitjà-alt. El procés d'AO resulta ser el menys efectiu, especialment en emprar l'ànode de Pt.

Mesures espectrofotomètriques van permetre el seguiment de la decoloració. Els processos EF i PEF mostren el mateix comportament, arribant a la pèrdua completa de color en l'escala de minuts. El procés d'AO presenta una activitat més pobre; la decoloració completa només és assolida després de vàries hores d'electròlisi o, en algún cas, ni tan sols assolida.

Àcids carboxílics de cadena curta i ions inorgànics van ser detectats alhora que quantificats emprant tècniques d'HPLC. Els àcids oxàlic i oxàmic són els principals àcids carboxílics detectats als processos EF i PEF, mentre que a l'AO només es troben breument en petites concentracions. Els ions NH_4^+, NO_3^- i SO_4^{2-} es van detectar en solució. NH_4^+ és l'espècie de nitrògen majoritària a EF i PEF; NO_3^- ho és per a l'AO. Tots els àtoms de sofre continguts a la molècula d'AR1 s'alliberen com a SO_4^{2-} per als tres processos evaluats.

La principal conclusió és que els EAOPs testats es manifesten com a processos nets, senzills i potents per degradar molècules aromàtiques complexes com l'AR1.

Paraules clau: Processos electroquímics d'oxidació avançada, electro-Fenton, fotoelectro-Fenton, oxidació anòdica, tractament d'aigües, diamant dopat amb bor, Acid Red 1.

3. INTRODUCTION

During decades scientific community has focused its efforts in the study of chemical pollutants whose presence in the environment has been or is regulated in several developed countries legislations. They can be identified as often nonpolar, toxic, persistent and bioaccumulative pollutants, such as polycyclic aromatic hydrocarbons (PAHs), polychlorinated biphenyls (PCBs) or dioxins.

Nonetheless, development of more sensitive analytical techniques has allowed the detection of other potentially toxic pollutants. The so-called emerging contaminants (ECs) are defined as pollutants previously unknown or not such recognized whose presence in the environment is not necessary new but it is the concern about the consequences they could result in [1].

They usually are compounds with high metabolic activity, so they can cause a big impact in low concentration. Moreover they are continuously spilled into the water cycle, widening the possibility of pollution even not being long-lasting or accumulative pollutants. Polybrominated diphenyl ethers (PBDEs), perfluorinated or alkylphenol ethoxylate surfactants, chlorinated paraffins, pesticides, aromatic dyes, drugs or drugs of abuse are some of these ECs which need high doses of research about their detection, impact and removal from environment.

This work is focused on aromatic azo dyes. They represent about 65 % of the total dye production worldwide [2], which is estimated to be over 700 000 tons in 2008 [3]. They are mainly used in textile industry and paper industry. A significant amount of wastewater is generated from these industries and discharged into the environment, more specifically water bodies like rivers and lakes. This causes a great problem of water coloration affecting light-dependant aquatic life, and generates environmental concern.

Despite the lack of toxicological information about azo dyes due to its high variety, some works already report mutagenic [2,4] and carcinogenic [5,6] activity caused by these compounds. Its persistence is also a reason of concern: they are stable in environmental conditions and not easily photodegraded. Common sewage treatment plants are not efficient in their removal, and usually generate non-desirable sludge [7].

Advanced oxidation processes (AOPs) are emerging and powerful processes which have demonstrated great capability to oxidize organic pollutants [3,8,9] present in the environment. They all are based in *in situ* generation of hydroxyl radical (•OH), the most oxidizing chemical known after fluorine. Its high standard reduction potential ($E°(•OH/H_2O)$ = 2.80 V) allows non-selective degradation of pollutants to dehydrogenated and hydroxylated species, which are mineralized to CO_2, H_2O and inorganic ions [3]. In this work electrochemical advanced oxidation processes (EAOPs) are presented. They stand out for being efficient, clean, environmental friendly and allowing work in mild conditions.

The simplest EAOP is anodic oxidation (AO). It is based upon mediated oxidation through heterogeneous •OH formed at the anode surface from water discharge reaction:

$$M + H_2O \rightarrow M(•OH) + H^+ + e^- \quad (1)$$

This process highly depends on anodic material nature. According to proposed theoretical models [10,11] two types of anodes can be described:

(a) Active anodes are those presenting great affinity in adsorbing •OH onto its surface (chemisorption) through reaction (2), and thus having low reactivity against organic compounds oxidation. Graphite, IrO_2, RuO_2 or Pt anodes are considered “active” retaining •OH on its surface (poor in the oxidation process).

$$M(•OH) \rightarrow MO + H^+ + e^- \quad (2)$$

(b) Non-active anodes are those presenting low surface affinity for •OH (physisorption), and then allowing its reduction against organic compounds through reaction (3). PbO_2 and boron-doped diamond (BDD) anodes are considered “non-active” (and then allow better organic combustion)

$$M(•OH) + R \rightarrow MO + CO_2 + H_2O + H^+ + e^- \quad (3)$$

Fenton’s reaction chemistry can be coupled to AO process to improve its efficiency [12]. The so-called electro-Fenton (EF) process is based in •OH additional generation through Fenton’s reaction:

$$Fe^{2+} + H_2O_2 + H^+ \rightarrow Fe^{3+} + •OH + H_2O \quad (4)$$

Generated hydroxyl radical in the bulk of the solution reacts then through two main parallel reactions:

$$Fe^{2+} + •OH \rightarrow Fe^{3+} + OH^- \quad (5)$$

$RH + {}^{\bullet}OH + H_2O \rightarrow ROH + H_3O^+$ (6)

Oxidation of Fe(II) (5) turns out to be an unproductive reaction. At the same time, •OH reacts indiscriminately with almost any kind of organic matter through reaction (6), that evolves into complete oxidized, i.e. mineralized organic compounds. To minimize the non-desired effect caused by reaction (5), Fe^{2+} is always added in small quantities.

In addition, in EF process H_2O_2 is constantly electrogenerated in reaction medium via the two-electron cathodic reduction of oxygen in acidic conditions:

$O_2 + 2H^+ + 2e^- \rightarrow H_2O_2$ (7)

Additional bulk-generated •OH through Fenton's reaction (4) increases oxidizing power of the whole process in an undivided cell. Furthermore, electro-Fenton's method yields higher efficiency than classical Fenton's reaction thanks to Fe(III) reduction in the cathode:

$Fe^{3+} + e^- \rightarrow Fe^{2+}$ (8),

regenerating Fe(II), which feeds reaction (4) acting as catalyst more than as reagent.

Nonetheless, it has been previously reported [13-15] the presence of some recalcitrant compounds, mainly carboxylate iron (III) complexes, hardly oxidized by •OH in EF processes. It is known that these complexes can be easily photolyzed under UV radiation [16]:

$Fe(OOCR)^{2+} + h\nu \rightarrow Fe^{2+} + CO_2 + R^{\bullet}$ (9)

Given that, radiation with UVA light in photoelectron-Fenton method (PEF) permits enhancement of the mineralization process. Besides, light has also a catalytic effect allowing regeneration of Fe(II) via the photoreduction of $Fe(OH)^{2+}$, the predominant Fe(III) specie in acidic conditions [13]:

$Fe(OH)^{2+} + h\nu \rightarrow Fe^{2+} + {}^{\bullet}OH$ (10)

At the same time, reaction (10) contributes with an extra supply of •OH having a synergic effect into the whole process.

4. OBJECTIVES

In this work a comparison is made between the three above mentioned methods when applying them against the azo dye Acid Red 1 (AR1), widely applied in wool and leather industry. Information regarding AR1 can be found in Appendix 1.

The main objective was to test the effectiveness of each method to degrade the dye in solution at laboratory scale. For this purpose, electrolytic experiments have been carried out to assess three different aspects that help to quantify their performance:

(a) Mineralization: The quantification and further comprehension of the mineralization process is of crucial importance to assess the capacity of each one of the methods to degrade organic matter. The objective here was to know what levels of mineralization could be reached depending on the method applied, and how are they modified when changing system parameters, e.g. testing several current densities and using anodes considered active or non-active.

(b) Decolouration: The study of decolouration process allows understanding of how the dye behaves in the initial stages of the electrolysis, besides giving direct information about how quickly colour is removed from the solution. Again, modification of electrolysis parameters was scheduled to take deeper insight in the process and understand how those changes affect it.

(c) Released species: The detection of organic and inorganic species found during electrolysis permits to know what is the fate of the dye molecule depending on the process performed. Concentration of inorganic ions and short-chained carboxylic acids change during electrolysis, and how it changes gives light about how different the three methods work.

5. EXPERIMENTAL

5.1. CHEMICALS

Commercial 60 % Acid Red 1 was supplied by Sigma-Adrich. Analytical grade anhydrous sodium sulphate and iron(II) sulphate heptahydrate were obtained from Fluka and Sigma-Aldrich, respectively. Organic solvents and other chemicals used in chromatographic techniques were of HPLC and analytical grade from Aldrich, Lancaster, Merck and Panreac. All water used in experimentation was high-purity, supplied by a Millipore Milli-Q system with resistivity > 18 MΩ cm at 25 °C.

5.2. ELECTROLYTIC PROCEDURES

Electrolytic experiments were performed in an open and undivided cell of 150 mL with an external jacket allowing circulation of thermostated water using a Selecta Digiterm 3000524. The BDD anode was provided by Adamant Technologies and Pt sheet anode of 99.99% purity was supplied by SEMPSA; the cathode was a carbon-PTFE air-diffusion electrode from E-TEK, allowing *in situ* H_2O_2 generation from air at 300 mL min^{-1} flow rate. All electrodes had a geometric area of 3 cm^2. Galvanostatic conditions were achieved with an Amel 2053 potentiostat-galvanostat.

All experiments were performed over 100 mL of solutions containing 236 mg L^{-1} AR1 (equivalent to 100 mg L^{-1} of total organic carbon (TOC)) 0.05 M Na_2SO_4 as background electrolyte and 0.5 mM Fe^{2+} as catalyst in EF and PEF cases, at pH 3. Thermostated solution was maintained at 35.0 °C, the maximum temperature found acceptable without significant water evaporation during prolonged electrolysis time. The solution was stirred via a magnetic bar spinning at 800 rpm to ensure homogeneity in solution. A Philips 6-W black light blue tube lamp was used for UVA irradiation in PEF case, providing light in 320-400 nm region with an energy of 5 W m^{-2}, as detected with a Kipp&Zonen CUV 5 global UV radiometer.

5.3. ANALYTICAL PROCEDURES

Solution pH was measured with a Crison GLP 22 pH-meter. The decolourization of solutions was measured using a Shimadzu 1800 UV-Vis spectrophotometer. Mineralization was monitored with a Shimadzu TOC-VCSN analyzer. TOC measurements are accomplished by complete conversion of carbon content in solution into CO_2 at 680 °C, followed by IR quantification of the CO_2 formed through a non-dispersive infrared analyzer. The equipment yields the value as total carbon (TC), which represents the addition of organic plus inorganic carbon in solution; given the acidic nature of the samples, inorganic CO_2 was taken as negligible. Then, direct measurements of TC were ascribed to CO_2 coming only from organic matter. Total nitrogen content was measured with a Shimadzu TNM-1 module coupled to Shimadzu TOC-VCSN analyzer. TN refers to organic nitrogen, ammonium, nitrate and nitrite contained in solution. Similarly to TOC, TN measurements are accomplished through total and indiscriminate combustion of nitrogen to NO and NO_2. Those nitrogen species are then reacted with O_3 to form an exited state of NO_2. Light energy is emitted upon returning to ground state, and then a chemiluminiscence detector is used to measure TN content.

Carboxylic acids were detected and quantified by injecting 20 mL aliquots into an ion-exclusion HPLC system using a Water 600 LC fitted with a Bio-Rad Aminex HPX 87H, 300×7.8 mm (i.d.), column coupled with a Waters 996 photodiode array detector at λ = 210 nm, with a mobile phase of 4 mM H_2SO_4 at 0.6 mL min^{-1}. Inorganic ions were detected by ionic chromatography using a Shimadzu 10 Avp HPLC coupled with a Shimadzu CDD 10 Avp conductivity detector. The NH_4^+ concentration was determined with a Shodex IC YK-421, 125×4.6 mm (i.d.), column at 40 °C, whereas SO_4^{2-} and NO_3^- content was quatified with a Shim-Pack IC-A1S, 100×4.6 mm (i.d.), column at 40 °C. These analysis were performed with 25 mL aliquots using a mobile phase containing 5.0 mM tartaric acid, 1.0 mM dipicolinic acid , 24.2 mM boric acid and 1.5 mM crown ether at 1.0 mL min^{-1} for the cation and 2.4 mM tris(hydroxymethyl)aminomethane and 2.5 phthalic acid at 1.5 mL min^{-1} for the anions.

6. MINERALIZATION OF ORGANIC MATTER

6.1. COMPARATIVE TOC REMOVAL OF AR1 SOLUTION BY AO, EF AND PEF PROCESSES

Understanding mineralization as the process by which organic matter turns into inorganic species, like CO_2, H_2O, SO_4^{2-}, NO_3^-, NH_4^+, etc. TOC experiments became a useful technique for quantification of this process, allowing measurements of how much organic carbon content is present in a sample.

A comparative study monitoring TOC removal in 0.5 mmol L^{-1} AR1 solution (equivalent to 100 mg L^{-1} TOC) has been carried out under AO, EF and PEF conditions using Pt and BDD as anode materials. All three processes have been performed in galvanostatic conditions, at pH 3, with an applied current density of 100 mA cm^{-2}, and with continuous stirring ensuring transport of species from/towards the electrodes.

Figure 1 shows TOC abatement for the three mentioned processes. AO curves clearly remarks the different behaviour between the anode materials. AO-Pt curve shows that TOC content of the solution is barely reduced during the whole process: there is still more than 80 % of organic matter after 6 h of experiment. Then, Pt anode itself virtually allows no mineralization of the total organic compounds present in the medium, supporting the thesis that classifies it as "active" anode (remember active anode is that which possess high affinity for $^{\bullet}OH$, then hindering its activity as oxidizing agent, reaction (2)).

On the other hand, the curve which represents TOC decay while using a BDD anode shows much higher grade of TOC abatement, with continuous decay in the course of the experiment and reaching almost 5 % of remaining organic carbon in solution at the end of it. Taking BDD as an example of "non-active" anode, it is clear, in mineralization terms, the difference between the two types of anodes, the former having almost no effect in mineralization of organic matter and the latter having a slow but constant mineralization activity, yielding practically total mineralization at the end of the process (6 h).

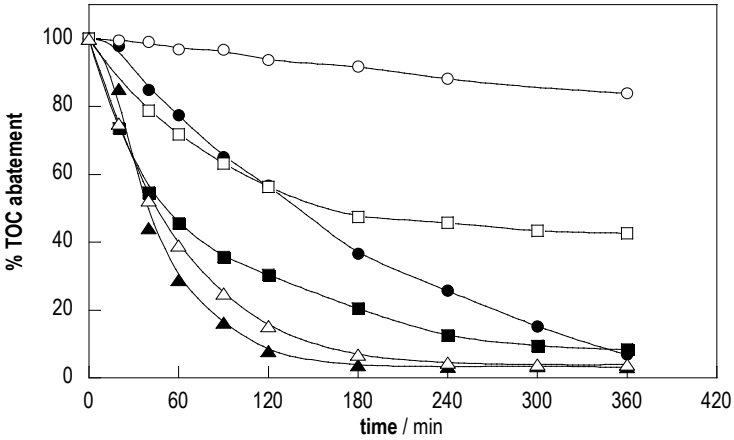

Figure 1. % TOC abatement vs. electrolysis time for 100 mL of 236 mg L^{-1} AR1 solution in 0.05 M Na_2SO_4, with 0.5 mM Fe^{2+} (only □,■,△,▲), pH 3.0, at 100 mA cm^{-2} for AO (○,●), EF (□,■) and PEF (△,▲) methods when using Pt (○,□,△) and BDD (●,■,▲) anodes.

The rest of the curves shown in Figure 1 represent the behaviour of TOC abatement during the course of EF and PEF processes. Initial concentration of Fe(II) in the working solutions for both methods was chosen to be 0.5 mmol L^{-1}, having performed previous experiments that aim at this concentration as the optimum.

The first EF curve shows TOC decay during performance of EF process using a Pt anode. As can be seen, behaviour at the beginning of the experiment is quite different from the one of the couple AO-Pt. During the first 2 h, TOC abatement only represents approx. 6 % of initial TOC in AO-Pt experiment, while it reaches more than 40 % for EF-Pt experiment. Given that the only difference between the two methods is the presence of •OH in solution (reaction (4)), it is quite clear that this 6-fold improvement achieved in the initial steps of the mineralization process is mainly caused because of the presence of the radical in solution.

Nevertheless, when EF-Pt couple is compared with AO-BDD, a similar TOC abatement is observed between them within the first 120 min, reaching both 42 % of mineralization degree. On the other hand, curve begin to diverge from 120 min on, leading to a final TOC abatement of 53 % in EF-Pt experiment, much lower than 95 % reached in AO-BDD. Although the initial behaviour could suggest similar mineralization power between them, it is clear that the two processes evolve through different pathways. This will be confirmed below (see colour removal section). It is also remarkable the asymptotic behaviour of EF curve, with only 4 % of

mineralization achieved during the last 3 hours, against the pseudo-linear behaviour of AO curve, showing approx. 12 % of mineralization per hour.

The second EF curve, representing the performance of EF-BDD couple, presents a much higher decay in the very initial steps than the others discussed to the moment. This can be assigned to the cooperative oxidizing power of •OH generated at BDD anode surface plus •OH generated at the bulk of the solution through reaction (4). 94 % of total TOC consumed after 6 h of experiment compared with 53 % for EF-Pt may suggest the great capability of BDD(•OH) to oxidize recalcitrant species generated in solution.

The last two curves, corresponding to PEF processes, clearly represent the fastest TOC abatement of all of them. A 85 % of TOC decay is achieved in PEF-Pt conditions after 120 min of experiment, becoming 93 % at half experiment (180 min) and finally reaching 96 %. PEF-BDD works even faster, reaching 92 % of TOC abatement at 120 min, 96 % at 180 and 97 % at the end of the experiment. The difference between EF-Pt and PEF-Pt couple can be explained by photolysis of Fe(III) complexes in PEF-Pt, turning faster its mineralization [14,15,17].

Given the similarity of the two PEF curves, it can be said that anode material is not crucial in PEF process. The mineralization power of bulk •OH combined with photolytic activity of UVA light make PEF the fastest and more effective of all of the six methods performed.

6.1. EFFECT OF CURRENT DENSITY

Current density *j* is a decisive parameter in all of the EAOPs exposed. The amount of hydroxyl radical generated in any of the processes depends directly on it, so it limits the mineralization rate at which each process evolves. Several experiments have been carried out to study current density influence over TOC abatement: a 0.5 mmol L^{-1} AR1 solution has been exposed to 6 h electrolysis using BDD anode and air-diffusion C/PTFE cathode for each of the three methods, using 4 different density currents (16.7, 33.3, 66.7 and 100 mA cm^{-2}) in each of them.

For all processes, the highest density current leads to the fastest TOC removal. Figure 2a shows the TOC decay curves for AO process. It can be noted a steady decrease of TOC content during the whole experiment. This indicates constant mineralization rates during all stages in mineralization process. It also can be noted a steady increase in TOC abatement from

lowest density current to highest during the whole process, percentages of mineralization reached in 6 h being 54 % for 16.7, 58 % for 33.3, 75 % for 66.7 and 92 % for 100 mA cm^{-2}.

Figure 2b shows TOC curves from EF process sampling. As in AO, the highest mineralization achieved corresponds to the highest current applied. After 6 h, relative values of TOC abatement are 68, 81, 87 and 92 % for 16.7, 33.3, 66.7 and 100 mA cm^{-2} respectively.

Although EF is more powerful than AO (for example, at 180 min mineralization reaches 61, 71, 75 and 80 % for EF and 25, 36, 46 and 63 for AO when *j* is 16.7, 33.3, 66.7 and 100 mA cm^{-2} respectively), it should be noted a big difference in curve behaviour: while in AO curves seem to follow some linearity during the whole experiment, in EF curves follow an abrupt decay at the beginning that is progressively softening to reach asymptotic behaviour at the end. This suggest again the accumulation of recalcitrant compounds formed thanks to Fe(III) presence, oxidized at a very slow rate when •OH is only present in the medium.

Figure 2c shows that all curves for PEF process follow the same behaviour as EF, caused by the presence of Fe(III) in solution. However, it can also be pointed a general better performance of the process compared to EF. PEF curves reach 84, 81, 91 and 96 % of mineralization when *j* is 16.7, 33.3, 66.7 and 100 mA cm^{-2}, respectively, after 180 min. Moreover PEF is the only method leading to almost total mineralization for all *j* tested at the end of each experiment, being the most powerful one between all of them.

It is clear then that higher current density yields higher mineralization for a given time, whatever method is tested. However, 16.7 and 33.3 mA cm^{-2} curves in PEF experiments have an almost identic behaviour; this suggests 16.7 mA cm^{-2} experiment yields the same mineralization level with less current, then being more efficient. Then, raw data shown in Figure 3 does not reflect if the highest current densities tested are also the most efficient.

For a better understanding of current density effect over the mineralization process, mineralization current efficiency (MCE) has been estimated for the experiments mentioned above. The equation used for this purpose compares the amount of mineralized organic matter against the theoretical mineralization that could be achieved ideally according Faraday's law:

$$MCE\ (\%) = \frac{nFV_s\Delta(TOC)_{exp}}{4.3234 \times 10^7\ mIt} \times 100 \qquad (1)$$

Where *F* is the Faraday constant (96487 C mol^{-1}), V_s is the solution volume (L), $\Delta(TOC)_{exp}$ is

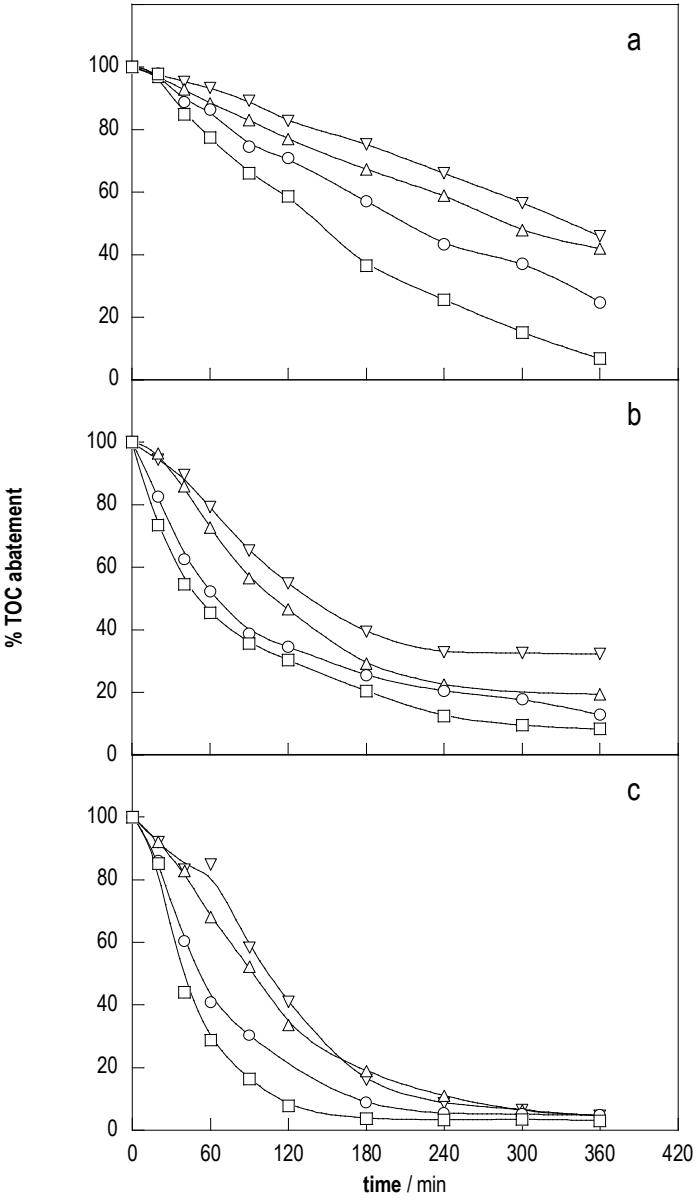

Figure 2. % TOC abatement vs. electrolysis time for 100 mL of 236 mg L^{-1} AR1 solution in 0.05 M Na_2SO_4, with 0.5 mM Fe^{2+} (only in b,c), at pH 3.0 at (▽) 16.7 mA cm^{-2}, (△) 33.3 mA cm^{-2}, (○) 66.7 mA cm^{-2}, (□) 100 mA cm^{-2} for (a) AO, (b) EF and (c) PEF methods.

the experimental TOC decay (mg L^{-1}), 4.3234 × 10^7 the conversion factor for unit homogenization (3600 s h^{-1} × 12011 mg mol^{-1}), *m* is the number of carbon atoms of AR1 (18 carbon atoms), *I* is the applied current (A) and *t* is the electrolysis time (h). The symbol *n* refers to the number of electrons involved in the theoretical complete combustion of AR1 through the following equation:

$$C_{18}H_{13}N_3O_8S_2^{2-} + 36H_2O \rightarrow 18CO_2 + 2SO_4^{2-} + 3NH_4^+ + 73H^+ + 74e^- \quad (11)$$

where SO_4^{2-} ions are expected as oxidation products of sulphonic groups, as well as NH_4^+ ions are from N contained in the molecule [17].

Figure 3 shows the results obtained from these calculations. At first glance it can be noticed the different behaviour of curves between AO (Figure 3a) and together EF and PEF processes (Figure 3b and c, respectively). In Figure 3a, the four curves appear to have similar behaviour. Except for the first moments of experiment, efficiency values tend to maintain in a given range, without great increase/decrease during electrolysis time. Then, AO seems to offer constant efficiency during the whole process.

However, two different series of values can be distinguished. Those corresponding to 50 and 100 mA exhibit bigger mineralization efficiency (9-12 % range) than those corresponding to 200 and 300 mA (around 4%). Note that 100 mA curve slightly tends to diminish from 3 h on.

This behaviour seems to be contradictory with that observed for TOC abatement. The latter suggests higher production of hydroxyl radical when increasing current density, which translates into higher mineralization rates. However, decrease in MCE aims to the existence of parasitic processes which compete with the desired one. Increasing potential when increasing *j* promotes non-desirable reactions which consume •OH physisorbed onto the anode surface, the main one following oxygen evolution [4,17]:

$$2BDD(^\bullet OH) \rightarrow 2BDD + O_2 + 2H^+ + 2e^- \quad (12)$$

In addition, other reactions cap hydroxyl radical generation in the anode through the production of weaker oxidants, like $S_2O_8^{2-}$ (13) and O_3 (14):

$$2SO_4^{2-} \rightarrow S_2O_8^{2-} + 2e^- \quad (13)$$

$$3H_2O \rightarrow O_3 + 6H^+ + 6e^- \quad (14)$$

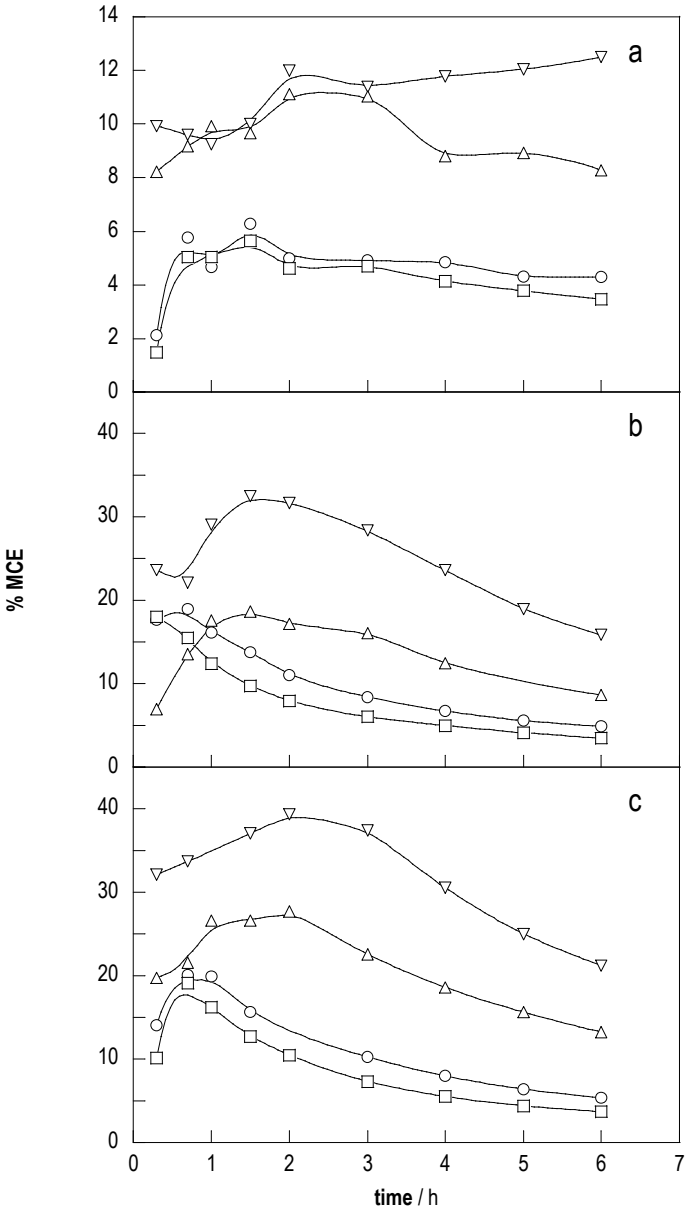

Figure 3. MCE calculations vs. electrolysis time for 100 mL of 236 mg L^{-1} AR1 solution in 0.05 M Na_2SO_4, with 0.5 mM Fe^{2+} (only in b,c), at pH 3.0 at (▽) 16.7 mA cm^{-2}, (△) 33.3 mA cm^{-2}, (○) 66.7 mA cm^{-2}, (□) 100 mA cm^{-2} for (a) AO, (b) EF and (c) PEF methods.

The same pattern is observed in Figure 3b and c, where highest MCE values correspond to lowest current densities. In these cases, though, curve behavior is quite different from the exposed above. The highest MCE values are achieved during the first moments of experiments, reaching values of 33 and 37 % MCE at 90 min for 16.7 mA cm^{-2} in EF and PEF respectively, then falling to lower values (24 and 31 % at 240 min) as time goes on. This fall is even quite fast for 200 and 300 mA cm^{-2} on both EF and PEF processes, going respectively from 19 and 20 % MCE at 40 min to 7 and 8 % at 240 min when *j* is 66.7 mA cm^{-2}.

Several reasons explain this behavior. As in AO case, parasitic oxygen generation (12) is promoted at high current densities. However, other important parasitic processes take place in EF and PEF methods. Hydroxyl radical from the bulk can dimerize to yield H_2O_2 (15) and then slow down Fenton's reaction (4), and •OH can also react against H_2O_2 to yield HO_2• (16), with lower oxidizing capacity than •OH:

$$2\bullet OH \rightarrow H_2O_2 \quad (15)$$

$$\bullet OH + H_2O_2 \rightarrow HO_2\bullet + H_2O \quad (16)$$

Moreover, H_2 evolution (17) is also promoted in the cathode, then reducing its capacity to electrogenerate H_2O_2:

$$2H^+ + 2e^- \rightarrow H_2 \quad (17)$$

Rapid decrease of organic matter in EF and PEF processes also contributes to MCE decrease, given that current density remains constant but organic matter in solution diminishes over time. Besides, accumulation of recalcitrant species in solution makes the process even much inefficient at final steps, where these are the main organic compounds present in the medium.

Slightly higher MCE values found for PEF process can be explained due to the photolytic component, not taken into account in the efficiency estimation.

7. COLOUR REMOVAL

7.1. COMPARATIVE COLOUR REMOVAL OF AR1 SOLUTION BY AO, EF AND PEF PROCESSES

Decolouration of dye solutions is also a key parameter for the study of dye degradation under AO, EF and PEF conditions. The rate at which colour disappears when applying the aforementioned methods gives valuable information about mechanisms involved in the whole mineralization process, then allowing deeper assessment upon them. It is important to remark that decolouration refers mainly to the compound of study (in this case AR1), and does not yield relevant specific information about other organics contained in solution

A comparative spectrophotometric study monitoring colour removal over 0.5 mmol L^{-1} AR1 solution has been carried out under AO, EF and PEF conditions using Pt and BDD as anode materials. All processes have been performed in galvanostatic conditions, at pH 3 and with continuous stirring ensuring transport of species from/towards the electrodes.

Expression (2) has been used for colour removal calculations:

$$CR\,(\%) = \frac{A_0 - A_t}{A_0} \times 100 \qquad (2)$$

Where A_0 and A_t represent absorbance measurements at initial time and electrolysis time t respectively, both at λ_{max} = 516 nm

Figure 4 shows colour removal versus electrolysis time for AO and EF methods at 100 mA cm^{-2} using Pt and BDD anodes. As can be seen, different performance in AO between Pt and BDD anodes it is relevant. Solutions treated with AO-BDD anode were completely decoloured at 180 min, while Pt only achieved 80 % of decolouration. Although not presented in Figure 4, Pt does not strictly reach complete decolouration, reaching 95 % of colour removal after 6 h of experiment. Furthermore, some differences are appreciable even in the decolouration rates. While AO-BDD reaches 45 % of decolouration at 30 min, AO-Pt barely reaches 19 %. This difference grows bigger at 90 min, when AO-BDD achieves 79 % of colour removal and AO-Pt only 54 %.

This behaviour difference can be ascribed to the main mechanisms promoted in each of the anodes, and so reinforces the thesis about active and non-active anodes: in Pt case, •OH radicals strongly chemisorbed on the electrode surface hardly oxidize the dye's azo bond and so is not able to completely decolour the solution. In contrast, when using BDD, a non-active

anode, physisorbed •OH reactivity is evidently enhanced, yielding total decolouration after half the time in which AO-Pt almost achieves it.

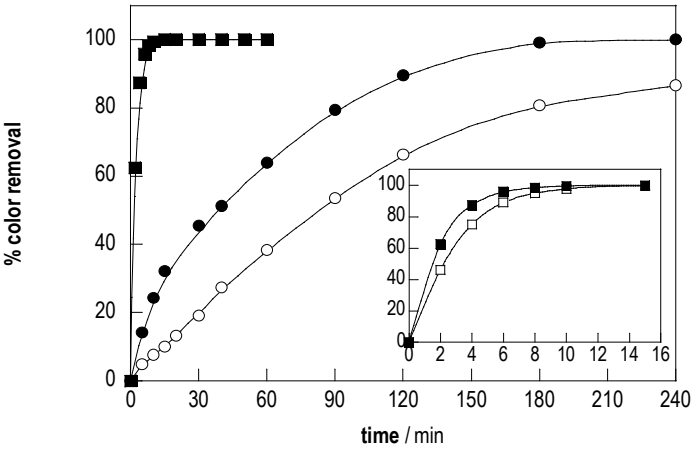

Figure 4. Percentage of color removal vs. electrolysis time for 100 mL of 236 mg L^{-1} AR1 solution in 0.05 M Na_2SO_4, with 0.5 mM Fe^{2+} (□,■), pH 3.0, at 100 mA cm^{-2} for AO (○,●) and EF (□,■) methods when using Pt (○,□) and BDD (●,■) anodes.

Nevertheless, EF process presented an appreciable higher decolouration rate than AO achieving complete colour removal in only 10 min of treatment whatever it is the nature of the anode. The addition of Fenton's chemistry to the process permits electrogeneration of •OH in the bulk as well as the anodic surface. Then, due to the big difference shown in Figure 4 between AO and EF, it is possible to say that •OH generated in the bulk is the main responsible for the rapid oxidation of AR1 in solution.

Even more, the comparison between Pt and BDD used in EF confirms that appointment. Inset panel in Figure 4 shows that EF-Pt couple evolve only slightly slower than EF-BDD couple, the former reaching complete decolouration only 5 min after the latter. Then, the azo bond breakage through bulk-generated •OH is the main process causing decolouration, with a little participation of the adsorbed •OH, higher on BDD as stated above.

In the case of PEF colour removal, under UVA light, it shows almost the same behaviour than the observed for EF process, as it is shown in Figure 5 for the treatment of AR1 solutions at 33.3 mA cm^{-2}.

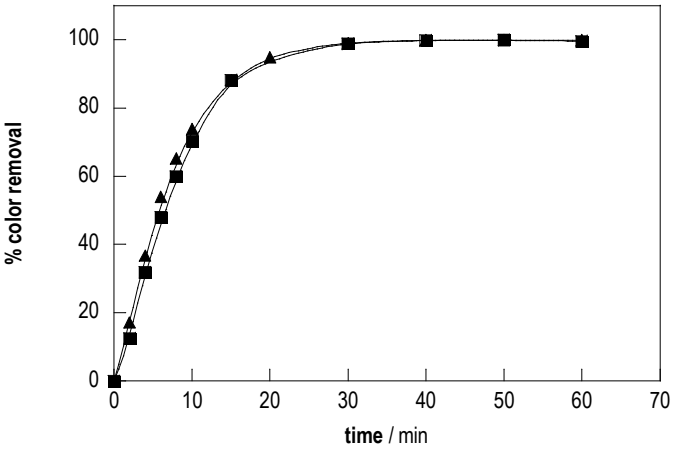

Figure 5. Percentage of color removal vs. electrolysis time for 100 mL of 236 mg L^{-1} AR1 solution in 0.05 M Na_2SO_4 with 0.5 mM Fe^{2+}, pH 3.0, at 33.3 mA cm^{-2} for EF (■) and PEF (▲) methods when using a BDD anode.

The two color removal curves are clearly overlapped, following nearly the same behaviour. These curves, beyond confirming the predominant oxidizing activity of bulk •OH, also point that there is no improvement in AR1 oxidation when UVA light is applied, because of expected AR1 photostability. Then, UVA light improvement in TOC removal can be only attributed to photolysation of intermediates during the mineralization process.

7.2. EFFECT OF CURRENT DENSITY

As in the case of TOC measurements, effect of current density has been studied for decolouration experiments using BDD as anode material. Figure 6 and 7 show percentage of colour removal for AO and EF methods respectively, at a current density of 100, 66.7 and 33.3 mA cm^{-2}. In both cases, colour fades out more rapidly when increasing current density through the system, as expected: the increase of *j* promotes higher generation of radicals (BDD(•OH)) in AO, plus •OH in solution in EF that increase degradation velocity and hence favour decolouration processes.

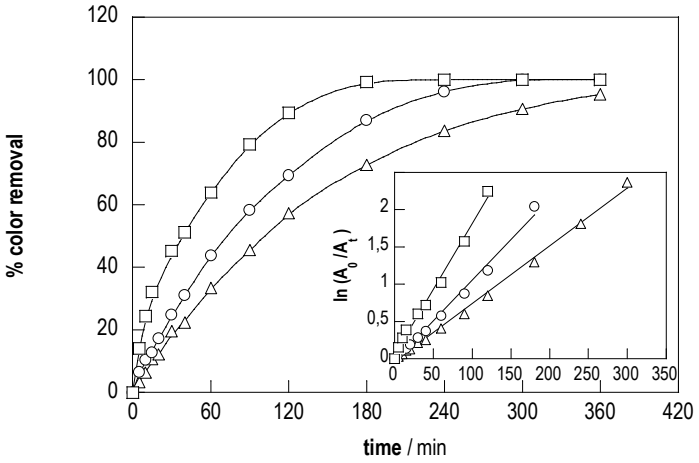

Figure 6. Percentage of color removal vs. electrolysis time for 100 mL of 236 mg L^{-1} AR1 solution in 0.05 M Na_2SO_4, pH 3.0, at (△) 33.3 mA cm^{-2}, (○) 66.7 mA cm^{-2}, (□) 100 mA cm^{-2} for AO method when using a BDD anode.

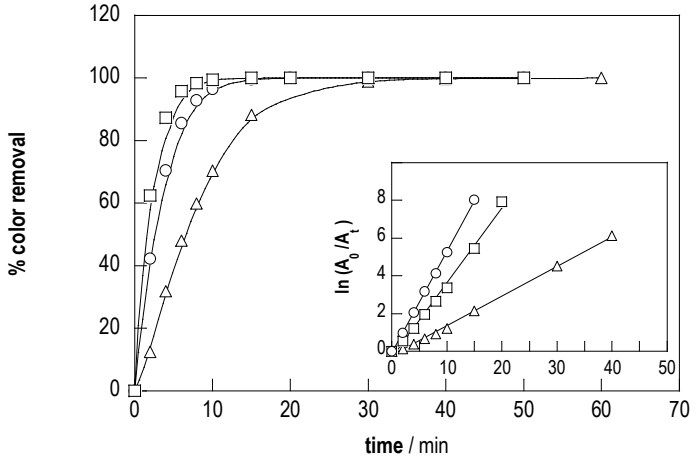

Figure 7. Percentage of color removal vs. electrolysis time for 100 mL of 236 mg L^{-1} AR1 solution in 0.05 M Na_2SO_4 with 0.5 mM Fe^{2+}, pH 3.0, at (△) 33.3 mA cm^{-2}, (○) 66.7 mA cm^{-2}, (□) 100 mA cm^{-2} for EF method when using a BDD anode.

In the AO case the increase in current density supposes a great decolouration improvement. Total decolouration is achieved at 180 min when a current 100 mA cm^{-2} current density is applied, while it is achieved at almost 300 min when applying 66.7 mA cm^{-2}, and it is not achieved at all for 33.3 mA cm^{-2}.

This is also the behaviour observed along the curves. Decolouration of 33 % is achieved at 60 min when applying 33.3 mA cm^{-2}, rising to 44 and 64 % when *j* is 66.7 and 100 mA cm^{-2}, respectively. It can be observed that the difference between 100 and 66.7 mA cm^{-2} curves is wider than that between 66.7 and 33.3 mA cm^{-2} curves. In fact, this difference is almost doubled in the former case respect the latter. This behaviour is maintained over time, values of colour removal reaching 57, 69 and 89 % when applying 33.3, 66.7 and 100 mA cm^{-2}, respectively, at 120 min.

In contrast, the pattern is reversed for the behaviour observed in EF experiments. For example, 12 % of decolouration is achieved at 2 min when applying 33.3 mA cm^{-2}, while 42 and 62 % are achieved for 66.7 and 100 mA cm^{-2} at the same time. In addition, this behaviour is remarked over time, given decolouration of 46, 85 and 95 % is achieved for 33.3, 66.7 and 100 mA cm^{-2}, respectively, at 6 min. The difference between the upper curves decreases and grows bigger between them and the lower.

This behaviour can be ascribed to the improvement achieved with the addition of Fenton's reaction (4) to the system. In the EF case, Fe^{2+} concentration in the medium is acting like a limiting reagent, given that its initial concentration cannot be exceeded during the process. Moreover, parasite reactions that diminish Fe^{2+} activity (5) are promoted at high current densities. These facts point to an approaching ceiling when increasing current density in EF that is not observed for AO case.

7.2.1. Decolouration rate

To better quantify and then clarify the effect of current density over decolouration level, decolouration rates have been calculated. It is important to note that decolouration rates cannot be strictly called decolouration kinetics due to the probable existence of coloured intermediates absorbing in the same wavelength than AR1. Then, reaction constants derived from these calculations must be called decolouration pseudoconstants, and have only experimental validity. The inset panels in Figure 6 and 7 show linear adjustment to first order kinetics for AO and EF

respectively. Following the modified first order linear equation, expressed in terms of absorbance, kinetic decolouration pseudoconstants can be easily calculated. :

$$ln\left(\frac{A_t}{A_0}\right) = kt \qquad (3)$$

Where A_0 and A_t represent absorbance measurements at initial time and electrolysis time t respectively, both at λ_{max} = 516 nm, k refers to first order decolouration pseudoconstant and t represents electrolysis time in seconds. Decolouration pseudoconstants are presented in Table 1. The difference between methods is quite clear, being EF constants one order of magnitude bigger than AO ones. The pattern observed in the decolouration curves is confirmed for the kinetics, given that numerical relations between them can be established as $2(k_{200} - k_{100}) \approx (k_{300} - k_{200})$ in AO case while $(k_{200} - k_{100}) > (k_{300} - k_{200})$ in EF case.

method	k_{100} [10^{-5} s^{-1}]	k_{200} [10^{-5} s^{-1}]	k_{300} [10^{-5} s^{-1}]
AO	0.7736 (0.997)	1.091 (0.991)	1.759 (0.993)
EF	15.72 (0.997)	39.51 (0.993)	53.60 (0.999)

Table 1. Decolouration pseudoconstant values at 33.3 (k_{100}), 66.7 (k_{200}) and 100 (k_{300}) mA cm^{-2} for AO and EF methods. Correlation coefficients are shown in parentheses.

7.3. EVIDENCE OF AROMATIC INTERMEDIATES

Spectra depicted in Figure 8 represent UV-Vis spectra recorded from AO (a) and EF (b) experiments carried out with BDD anode and a current density of 66.7 mA cm^{-2}. They confirm much faster decolouration for EF compared to AO. Two partially overlapped high-intensity bands can be observed around 516 nm, centred at 506 and 530 nm. Several bands can also be observed in UV zone; centred at 236, 252, 312, 324 and 364 nm, they present lower intensity as wavelength increases.

The evolution of both spectra is quite different. Figure 8a shows, besides the time needed to achieve complete decolouration, an assembly of spectra that uniformly loose intensity as time goes by. Then, AR1 represents the vast majority of molecules absorbing in 200-800 nm range, and so being the principal aromatic specie in solution during the whole process.

In contrast, spectra shown in Figure 8b have a much different aspect. The main bands located around 516 nm experience shortening and widening even after 2 min of electrolysis, growing shorter and wider as time increases. This behaviour is also observed for the bands at

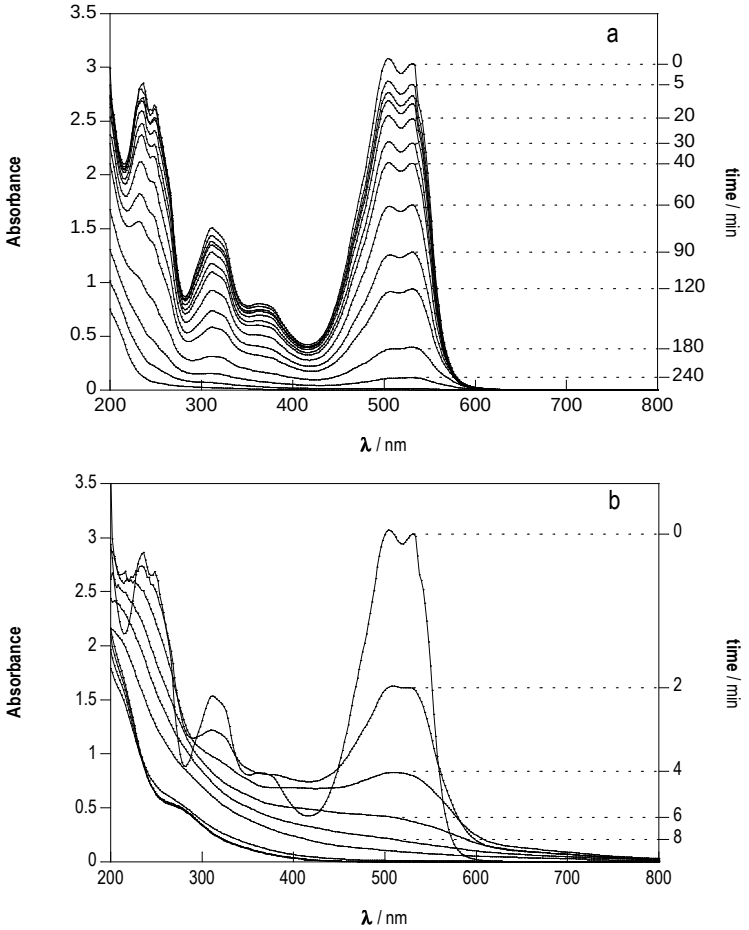

Figure 8. UV-Vis spectra recorded from AR1 solution in 0.05 M Na_2SO_4, pH 3.0, at 66.7 mA cm^{-2} (a) for AO method between 0 and 360 min of electrolysis and (b) for EF method between 0 and 60 min of electrolysis.

312 and 324 nm, in addition of fading and finally disappearing at 6 min. Spectrum recorded after 2 min of electrolysis doubles the absorbance recorded at initial time in the zone nearby 410 nm, and a new tiny band centred at 380 nm completely covers that centred at 364 nm. Absorbance also increases in 200-300 nm range. The band centred at 236 nm seems to grow more intense at 2 min, and progressively shifts towards 200 nm, completely disappearing at time higher than 10 min. An incipient band centred at 272 nm can be seen appearing at final

decolouration times. All these facts evidence a complex mechanism in solution, probably caused by the rapid formation and removal of smaller aromatics coming from AR1 degradation.

8. CHEMICAL SPECIES FOUND IN SOLUTION

8.1. EVOLUTION OF CARBOXYLIC ACIDS

It is well-known that short-chained carboxylic acids are generated from the cleavage of aromatic species under EAOPs treatment, and they form Fe(III) complexes when iron species are present [4,16]. Detection of these compounds gives deeper understanding of the processes involved and allow EAOPs coupling with other techniques, for example biological treatment, as they are biologically degradable.

The generation of carboxylic acids was comfirmed in AR1 solutions for all the methods performed, mainly for EF and PEF processes and for AO to a lesser extent. Experiments were carried out with a BDD anode at a current density of 100 mA cm^{-2}, monitoring carboxylic acids content by ion-exclusion HPLC chromatography. Several species were identified, being oxalic, oxamic, glycolic, formic and acetic acids (Figure 9) the most relevant ones, appearing at 6.9, 9.4, 12.2, 13.7 and 14.9 min retention times respectively.

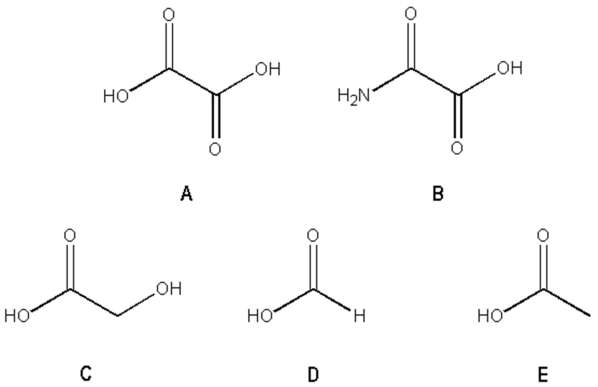

Figure 9. Molecular formulas of (A) oxalic, (B) oxamic, (C) glycolic, (D) formic and (E) acetic acids

In AO experiments little amount of these species were detected given that they are simultaneously degraded by BDD(•OH) and tend to accumulate in low extent. The most relevant one was glycolic acid, appearing at 20 min of electrolysis time and reaching a maximum concentration of 10.5 mg L^{-1} at 90 min. Other species detected in relevant amounts in this process include acetic and oxamic acids, appearing both at early electrolysis time and reaching their maximum at 180 min, with concentration of 8.0 and 4.1 mg L^{-1} respectively. Formic acid was also detected between 90 and 240 min, but only reaching a maximum of 1.2 mg L^{-1}. Maleic, succinic and acrylic acids were detected in an amount lesser than 1.0 mg L^{-1}, and disappeared quickly.

A different pattern was found for EF and PEF methods. Oxalic acid, not detected in AO experiment, was the main indentified carboxylic acid in both cases, reaching maximum concentrations of 89.3 and 79.6 mg L^{-1} for EF and PEF methods respectively (Figure 10). Oxalic acid is expected to be a very recalcitrant species [17] when Fe(III) is found in solution, since Fe(III) oxalate complexes are hardly oxidizable even with •OH, and then tend to form and accumulate, finding them in high concentration along the process.

Figure 10a shows oxalic acid evolution during electrolysis time for EF and PEF methods. In PEF case, the curve representing oxalic acid concentration behaves as expected. Despite early formation of the acid at early time, it also decays rapidly until it barely disappears at 180 min of electrolysis time. This can be ascribed to the photodecarboxylation process (9) that mineralizes iron(III) oxalate complexes by a ligand to metal charge transfer reaction promoted by UVA irradiation and additionally recovers Fe^{2+} to enter Fenton reaction (4).

To clearly see the implication of introducing UVA light into the process, EF and PEF experiments were carried out with a Pt anode at 100 mA cm^{-2}. Figure 10a shows oxalic acid evolution during electrolysis experiments. What can be seen in PEF method is mostly the same as observed when using BDD; oxalic acid reaches a maximum concentration of 125.7 mg L^{-1} at 40 min of electrolysis time, and then begins to fall rapidly until total disappearance at 300 min. The generation of acid that is slowly oxidized explains the achievement of a higher concentration level and then the time shift in the maximum and in the complete depletion of the species.

Instead, the lack of decarboxylation reactions is evident in EF curve. A maximum concentration of 105.5 mg L^{-1} oxalic acid is reached at 60 min, and a slowly decay follows which

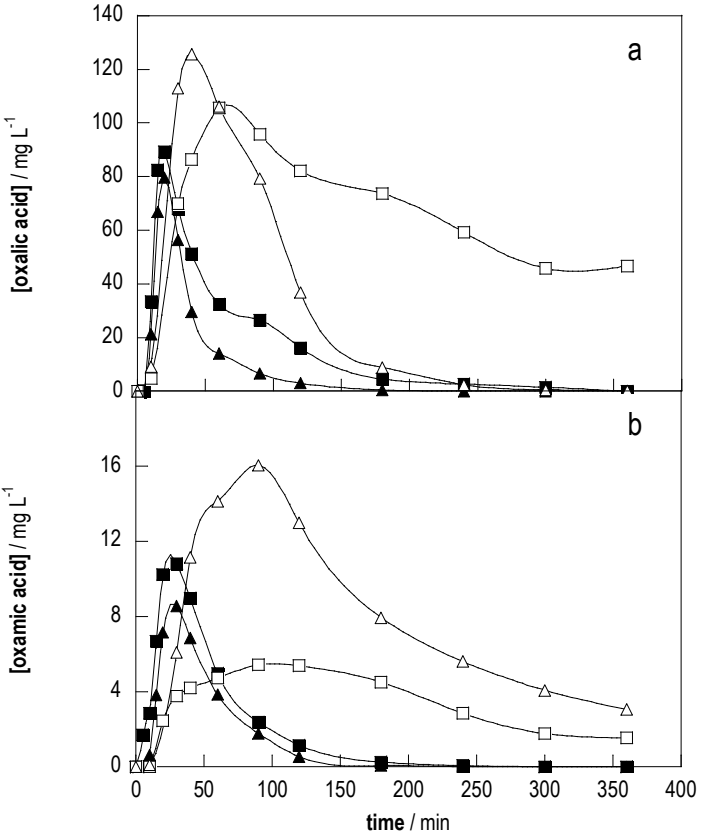

Figure 10. Evolution of (a) oxalic and (b) oxamic acids detected during 360 min of electrolysis of 100 mL of 236 mg L^{-1} AR1 solution in 0.05 M Na_2SO_4 with 0.5 mM Fe^{2+}, pH 3.0, at 100 mA cm^{-2} for EF (□,■) and PEF (△,▲) methods when using Pt (□,△) and BDD (■,▲) as anodes.

leads to a final concentration of 46.7 mg L^{-1}, that is a 49 % degradation over the maximum oxalic acid concentration achieved.

Besides oxalic acid, oxamic acid is also considered a recalcitrant species in EAOPs. It is a product from the cleavage of aromatic species containing N atoms, as is the case of aromatic azo dyes. Although generated in smaller amounts than oxalic acid, it also form Fe(III) complexes hardly oxidizable by •OH and BDD(•OH). Figure 10b shows the evolution of oxamic acid for both EF and PEF method, when using BDD and Pt as anode materials. In the BDD

cases, it is accumulated up to 10.8 and 8.5 mg L^{-1} at 30 min, following then a rapid depletion until total removal at 240 and 180 min for EF and PEF methods, respectively.

In the Pt cases, oxamic acid is much more rapidly produced in PEF than in EF, reaching 16.1 mg L^{-1} at the former and 5.4 mg L^{-1} at the latter, both at 90 min. However, it is also more rapidly removed; 1.8 and 3.0 mg L^{-1} oxamic acid left for EF and PEF respectively, at 360 min. The large amount of oxamic acid formed in PEF case can be related to the photolysis of several *N*-intermediates accelerating the production of oxamic acid, while the faster depletion can be ascribed to Fe(III) oxamate complexes photodecarboxylation by UVA light.

Other species like glycolic and acetic acids have been detected in EF and PEF experiments, always below 4 mg L^{-1}.

8.2. RELEASE OF INORGANIC IONS

Nitrogen and sulphur contained in AR1 molecule are also expected to be released as inorganic species, mainly as NH_4^+ and NO_3^- ions for N and as SO_4^{2-} ion for S. Ionic chromatography experiments confirmed the progressive generation of these species from AO, EF and PEF methods, as can be shown in Figure 11.

Figure 11a shows the evolution of released ammonium cation. All methods seem to generate a steady amount of NH_4^+ during the whole process, having AO the lowest discharge of NH_4^+ into the medium. A similar concentration of the species is generated from both EF and PEF until 90 min of electrolysis; at this point, NH_4^+ concentration in solution grows bigger for EF than for PEF. At final steps it is almost doubled in EF process regarding PEF, both reaching a plateau presumably caused because of the lack of more oxidizable *N*-intermediates in solution to be degraded.

Figure 11b shows two different patterns in NO_3^- concentration behaviour: one following a moderate and steady growth through all electrolysis time and another following a bigger growth in the initial stages which becomes a plateau from 90 min on. The first case corresponds to AO method, as seen for NH_4^+. The second case corresponds to EF and PEF methods. As similarly seen in Figure 11a, both follow the same behaviour up to 40 min, where EF curve continues to grow while PEF one evolves towards a plateau. A plateau is reached at 90 min for EF method.

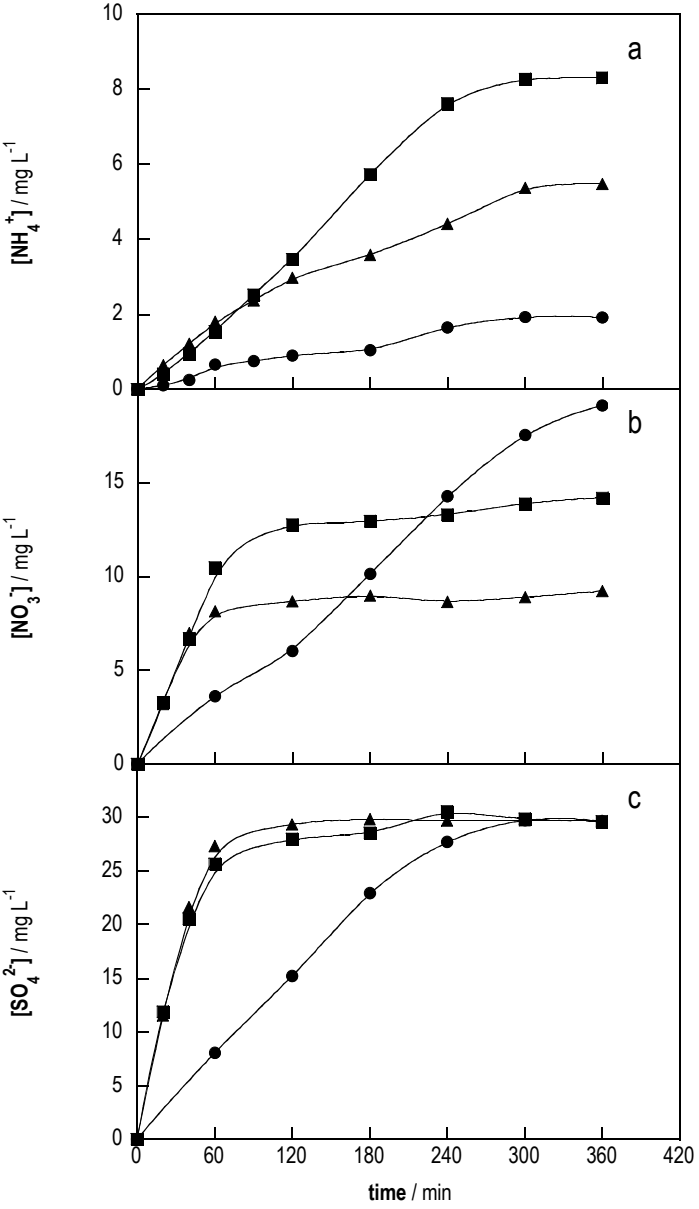

Figure 11. Evolution of (a) NH_4^+, (b) NO_3^- and (c) SO_4^{2-} ions detected during 360 min of electrolysis of 100 mL of 236 mg L^{-1} AR1 solution in 0.05 M $NaClO_4$, with 0.5 mM Fe^{2+} (■,▲), pH 3.0, at 100 mA cm^{-2} for AO (●), EF (■) and PEF (▲) methods when using a BDD anode.

The behaviour observed in both NH_4^+ and NO_3^- when AO conditions are applied fits well with that observed for TOC and colour removal. Release of *N*-containing ions is constant over time due to the continuous presence of AR1 as main compound present in solution.

Total nitrogen (TN) analysis was carried out at 360 min of electrolysis to assess final distribution of nitrogen initially contained in AR1 molecule. Table 2 contains experimental concentration (in mg L^{-1}) found for *N*-species as well as percentages indicating what fraction of initial nitrogen represents each one of them. TN values can also be found.

process	NH_4^+		NO_3^-		TN	
	mg L^{-1}	%	mg L^{-1}	%	mg L^{-1}	%
AO	1.9	7.6	19.1	22.2	18.1	93.0
EF	8.3	32.0	14.2	16.5	11.8	60.8
PEF	5.5	21.9	9.2	10.5	11.9	61.1

Table 2. Experimental concentrations (in mg L^{-1}) and % of initial nitrogen of NH_4^+ and NO_3^- ions, and total nitrogen (TN) content (in mg L^{-1} and % of initial nitrogen) found at 360 min of electrolysis for 100 mL of 236 mg L^{-1} AR1 solution in 0.05 M $NaClO_4$ with 0.5 mM Fe^{2+}, pH 3.0, at 100 mA cm^{-2}, under AO, EF and PEF conditions.

As can be seen in Table 2, some nitrogen is lost during electrolysis: almost 40 % in EF and PEF processes and only 7 % in AO. This loss can be ascribed to the formation of volatile *N*-species, like NO_x or N_2, not remaining in solution. NO_3^- is the main N ion released in AO, reaching 22 % of initial N, while NH_4^+ is the main N ion released in EF and PEF, reaching 32 and 22 % of total N contained in AR1. That is the reason why NH_4^+ has been used as complete-mineralization derivative in MCE calculations.

Assuming that no oxamic acid was left at 360 min for these experiments, NH_4^+ and NO_3^- are responsible of 30, 49 and 32 % of initial N for AO, EF and PEF respectively. Then, 63, 12 and 29 % are, respectively, the relative amount of N contained in solution at 360 min not assignable to any of the species mentioned above.

Figure 11c shows the evolution of SO_4^{2-} ion. As in the former case, a steady release of the ion is found for AO, while mainly all SO_4^{2-} in EF and PEF processes is released at first 60 min. This could suggest sulphonic groups present in AR1 are detached from the molecule at the

same time its degradation occurs, pointing at non-existence of sulphonated reaction intermediates. 29.6 mg L^{-1} SO_4^{2-} are released at 360 min for all the methods tested. This value matches exactly with the theoretical SO_4^{2-} concentration calculated from the cleavage of sulphonic groups, confirming that they are only mineralized to SO_4^{2-}.

10. CONCLUSIONS

EAOPs have proved to be a powerful tool to degrade Acid Red 1 in solution. The relative mild conditions at which those methods have been performed indicate the main role of hydroxyl radical as the main oxidizing agent in the system.

Boron doped diamond anode, an example of the so-called non-active anodes, has demonstrated to be an ideal material to carry out this kind of processes through physisorbed hydroxyl radical BDD(•OH). Platinum anode has shown its active anode nature yielding poor results in the degradation of AR1 solutions by itself.

Complete decolouration has been achieved for AO process in hour-scale when using BDD, while medium-high levels of mineralization have been reached. On the other hand, complete colour removal is not achieved and only 20 % of mineralization is reached when using Pt.

The coupling of Fenton's chemistry to the processes has improved greatly the results obtained. Electro-Fenton and photoelectro-Fenton methods have demonstrated to be more effective in both mineralization and decolouration of the solutions.

In those methods high levels of mineralization have always been reached, and total colour removal is achieved in minute-scale. Additional UVA radiation in photoelectron-Fenton method enhances the mineralization process; photolyzation of recalcitrant hardly-oxidyzable intermediate species generated from AR1 cleavage allows almost total mineralization of the solutions.

Short-chained acids have been detected in low concentration through anodic oxidation experiments. They are rapidly oxidized by BDD(•OH) species and tend not to accumulate. However, oxalic and oxamic acids are greatly found in electro-Fenton and photoelectron-Fenton experiments.

Hardly-oxidyzable oxalate and oxamate iron(III) complexes rapidly form to accumulate at initial electrolysis stages, then being rapidly oxidized in both methods until total depletion when using BDD.

When using platinum, electro-Fenton experiments are not able to completely degrade thoses species. UVA radiaton effect is clearly observed in this case due to complete degradation of oxalic acid in PEF process.

The effect of current density over EAOPs power has also been tested, showing for all methods that increase in *j* involves an increase in mineralization level and decolouration rate, but lowers the global efficiency of the processes through the promotion of non-desirable parasitic reactions.

Finally, all the results provided plus existent bibliographic information point at electrochemical advanced oxidation processes as an adequate, reliable and feasible alternative for wastewater treatment containing pollutants hardly removable with other techniques.

11. REFERENCES

1. Barceló, L.D.; López de Alda, M.J. Contaminación y calidad química del agua: el problema de los contaminantes emergentes. Fundación Nueva Cultura del Agua, technical report. http://www.fnca.eu/panel-cientifico-de-seguimiento-de-la-politica-del-aguas (accessed 12/03/13).
2. Carneiro, P.A.; Umbuzeiro, G.A.; Oliveira, D.P.; Zanoni, M.V.B. Assessment of water contamination caused by a mutagenic textile effluent/dyehouse effluent bearing disperse dyes, *J. Hazard. Mater.* **2010**, *174*, 694-699.
3. Martínez-Huitle, C.A.; Brillas, E. Decontamination of wastewaters containing synthetic organic dyes by electrochemical methods: A general review. *Appl. Cat. B-Environ.* **2009**, *87*, 105-145.
4. Ohe, T.; Watanabe, T.; Wakabayashi, K. Mutagens in surface waters: a review, *Mutat. Res.* **2004**, *567*, 109-149.
5. Platzek, T.; Lang, C.; Grohmann, G.; Gi, U.S.; Baltes, W. Formation of a carcinogenic aromatic amine from an azo dye by human skin bacteria in vitro, *Hum. Exp. Toxicol.* **1999**, *18*, 552-559.
6. Fieblinger, D.; Platzek, T. Genotoxicity studies with the colorant Acid Red 1, *Toxicol. Lett.* **2009**, *189*, S48-S49.
7. Robinson, T.; McMullan, G.; Marchant, R.; Nigam, P. Remediation of dyes in textile effluent: a critical review on current treatment technologies with a proposed alternative, *Bioresour. Technol.* **2001**, *77*, 241-255.
8. Chiron, S.; Fernandez-Alba, A.; Rodriguez, A.; Garcia-Calvo, E. Pesticide chemical oxidation: state-of-the-art, *Water Res.* **2000**, *34*, 366-377.
9. Klavarioti, M.; Mantzavinos, D.; Kassinos, D. Removal of residual pharmaceuticals from aqueous systems by advanced oxidation processes, *Eviron. Int.* **2009**, *35*, 402-417.
10. Comninellis, C.; De Battisti, A. Electrocatalysis in anodic oxidation of organics with simultaneous oxygen evolution, *J. Chim. Phys.* **1996**, *93*, 673-679.
11. Panizza, M.; Cerisola, G. Direct and mediated anodic oxidation of organic pollutants, *Chem. Rev.* **2009**, *109*, 6541-6569.
12. Brillas, E.; Sirés, I.; Oturan, M. Electro-Fenton Process and Related Electrochemical Technologies Based on Fenton's Reaction Chemistry, *Chem. Rev.* **2009**, *109*, 6570-6631.
13. Moreira, F.C.; Garcia-Segura, S.; Vilar, V.J.P.; Boaventura, R.A.R.; Brillas, E. Decolorization and mineralization of Sunset Yellow FCF azo dye by anodic oxidation, electro-Fenton, UVA photoelectro-Fenton and solarphotoelectro-Fenton processes, *Appl. Cat. B-Environ.* **2013**, *142-143*, 877-890.
14. C. Flox,C.; Garrido, J.A.; Rodríguez, R.M.; Cabot, P.L.; Centellas, F.; Arias, C.; Brillas, E. Mineralization of herbicide mecoprop by photoelectro-Fenton with UVA and solar light, *Catal. Today* **2007**, *129*, 29-36.
15. Garcia-Segura, S.; El-Ghenymy, A.; Centellas, F.; Rodríguez, R.M.; Arias, C.; Garrido, J.A.; Cabot, P.L.; Brillas, E. Comparative degradation of the diazo dye Direct Yellow 4 by electro-Fenton, photoelectro-Fenton and photo-assisted electro-Fenton, *J. Electroanal. Chem.* **2012**, *681*, 36-43.
16. Šima, J.; Makáňová, J. Photochemistry of iron(III) complexes, Coordin. *Chem. Rev.* **1997**, *160*, 161-189.
17. Garcia-Segura, S.; Brillas, E. Mineralization of the recalcitrant oxalic and oxamic acids by electrochemical advanced oxidation processes using a boron-doped diamond anode, *Water Res.* **2011**, *45*, 2975-2984.

12. ACRONYMS

AO	Anodic oxidation
AOP	Advanced oxidation process
AR1	Acid Red 1
BDD	Boron-doped diamond
EAOP	Electrochemical advanced oxidation process
EC	Emerging contaminant
EF	Electro-Fenton
HPLC	High performance liquid chromatography
MCE	Mineralization current efficiency
PEF	Photoelectro-Fenton
PTFE	Polytetrafluoroethylene
TC	Total carbon
TN	Total nitrogen
TOC	Total organic carbon

APPENDICES

APPENDIX 1: ACID RED 1

Chemical structure	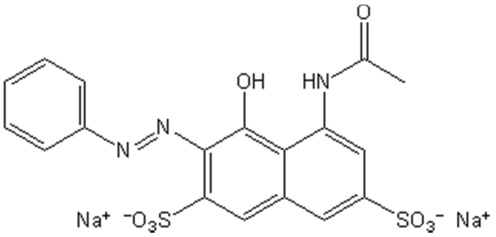
Chemical formula	$C_{18}H_{13}N_3Na_2O_8S_2$
IUPAC name	Sodium 5-(acetylamino)-4-hydroxy-3-(2-phenyldiazenyl)-2,7-naphthalenedisulfonate
Colour Index name	Acid Red 1
CAS number	3734-67-6
Colour Index number	18050
M [g mol^{-1}]	509.44
λ_{max} [nm]	516